Reconnection in Three Dimensions: The Role of Spines in Three Eruptive Flares

Angela Des Jardins[1], Richard Canfield[1], Dana Longcope[1], Crystal Fordyce[2] and Scott Waitukaitis[3]

[1] *Physics Department, Montana State University, Bozeman, MT 59717-3840, U.S.A.,*
[2] *Department of Physics and Astronomy, Clemson University, Clemson, SC, 29634, U.S.A.,*
[3] *Department of Physics, University of Arizona, Tucson, AZ, 85721, U.S.A.*

Submission: 1-24-2007

ABSTRACT

In order to better understand magnetic reconnection and particle acceleration in solar flares, we compare the RHESSI hard X-ray (HXR) footpoint motions of three flares with a detailed study of the corresponding topology given by a Magnetic Charge Topology (MCT) model. We analyze the relationship between the footpoint motions and a topological feature called spine lines and find that the examined footpoints sources moved along the spine lines. HXR footpoint motions predicted by standard 2.5D flare model *cannot* explain this relationship. We present a 3D model in which the movement of footpoints along spine lines *can* be understood. Our 3D model also explains other important properties of HXR footpoint motions that cannot be described by the standard model, such as the sense of their relative motions.

1. Introduction

Magnetic reconnection is the mechanism of topological change that is thought to bring about energy release and non-thermal electron acceleration in solar flares. By studying the radiative output of flares in association with the magnetic topology of the flaring region, we can learn a great deal about the topological location of reconnection. Knowing the location of reconnection is key to understanding both flare trigger and evolution processes.

Since the wealth of data now available from Ramaty High Energy Solar Spectroscopic Imager (RHESSI; Lin et al. 2002) exhibits many cases of hard X-ray (HXR) footpoint motion, an explanation for the various types of movement is of great interest. For example, Fletcher & Hudson (2002) compare observed footpoint motions to those predicted by flare models. They conclude that footpoint motions do not resemble the simple increase in separation expected in 2D reconnection models. For the 29 October 2003 X10 flare, Krucker et al. (2005) analyze the HXR footpoint velocity variations and the underlying photospheric magnetic field strength. They observe that the footpoint velocity is generally slower in the areas where magnetic field strength is higher. Bogachev et al. (2005) analyze the HXR footpoint motions of 31 flares observed by the *Yohkoh* Hard X-ray Telescope (HXT; Kosugi et al. 1991) with respect to neutral lines calculated from photospheric magnetograms. They find that only 13% of footpoints move away from the neutral line.

Several groups have sought to explain flare features via topological models. Gorbachev & Somov (1988) describe a topological model which satisfies the observational requirements of two-ribbon flares, such as HXR 'knots' in the ribbons. In their model, the active region separator, the special field line on which reconnection occurs, directs the released energy flux to the flare ribbons. Somov et al. (1998) present a reconnection model which explains the observation that the separation of HXR footpoints in 'less impulsive' flares (impulsive phase $t > 30$-40 s) tends to increase while in 'more impulsive' flares ($t < 30$-40 s), it decreases. They attribute the increase/decrease in footpoint separation to an increase/decrease in the longitudinal field at the flaring separator, increasing/decreasing the length of the reconnected field lines.

While substantial work has been done in the areas of multi-wavelength analysis of solar flares and coronal magnetic field modeling, little attention has been given to the combination of these two fields. Metcalf et al. (2003) describe a coincidence between magnetic separatricies and features of the 25 August 2001 white-light flare. They conclude that the HXR footpoint motions present in this flare are consistent with reconnection at a separator. Here, we explore three flares by examining the relationship between HXR footpoints and spine lines.

In this paper, for the first time, we compare flare HXR footpoint motions observed by RHESSI and a detailed study of the active region's magnetic topology. This examination is conducted using data from the Solar and Heliospheric Observatory's Michelson Doppler Imager (SOHO/MDI; Scherrer et al. 1995) and a magnetic charge topology model (MCT; see Longcope 2005). The MCT model allows us to observationally characterize the connectivity of coronal field lines by defining distinct source regions in the photosphere. We use this information to explain footpoint motions within the framework of magnetic reconnection – the transport of flux from one pair of sources to another – and flare models.

Several topological features are important to reconnection in flares (for terminology see Longcope 2005). *Poles* are the positive and negative point sources of magnetic flux, an idealization of well-defined features like sun spots and pores. The set of all field lines originating at a given positive pole and ending at a given negative pole fills a volume of space called a *domain*. A *separatrix* is a boundary surface dividing domains. *Null points* are the locations where the magnetic field vanishes. Near null points, the magnetic field is approximately

$$\boldsymbol{B}(\boldsymbol{x}_a + \delta\boldsymbol{x}) \approx \mathbf{J}^a \cdot \delta\boldsymbol{x}, \tag{1}$$

where $J^a_{ij} = \partial B_i/\partial x_j$ is the Jacobian matrix evaluated at x_a. This matrix has three eigenvalues which sum to zero because it must be traceless; $\boldsymbol{\nabla} \cdot \boldsymbol{B} = 0$. If two eigenvalues are positive (negative) then the null is positive (negative). The eigenvectors associated with the two like-signed eigenvalues define the *fan*, in which the separatrix field lines lie. The third eigenvector defines one parallel and one anti-parallel *spine* field line, which connect the null's two *spine poles*. A spine line usually lies in the photosphere, extending from a pole through a null to another pole of the same polarity. A *separator* field line, which starts and terminates at null points, is the intersection between separatrix surfaces. A separator is the generalization to three dimensions of a two-dimensional X-point. While reconnection can also occur on separatrix surfaces, separators are hypothesized to be the main location for reconnection in MCT models (Greene 1988; Lau & Finn 1990).

There are several advantages to this MCT method including: 1) Due to the fact that the topological features are quantitatively defined, powerful mathematical tools can be used. One of these tools is the ability to calculate the spine lines associated with the field. 2) Model sources represent the fluxes and locations of strong photospheric fields, thus the photospheric boundary of the model is a quantitative representation of the observed line of sight magnetogram. Extrapolating the complex magnetic field of flaring active regions into the corona using non-linear force free field models has yet to be accomplished. 3) Calculation of the topological features of the model coronal field is not computationally time consuming, so we are able to study several cases. Quasi-Separatrix Layers (QSLs) have been shown to be analogous to separatrix surfaces (see Démoulin 2006) and thus the intersection of QSLs with the photospheric surface are partially analogous to spine lines. However, the study of QSLs is currently limited because the numerical techniques required to compute the coronal fields are too limited (Démoulin 2006).

In this paper, we present the analysis of three X class flares, each well observed by RHESSI, each exhibiting significant footpoint motion. We have examined the HXR emission in detail (see Section 2), calculating the centroids of each footpoint source several times per minute, or as frequently as count statistics allowed. A MDI magnetogram close to each flare start time was used as an input to the MCT extrapolation model, resulting in a topological map of each flaring active region (see Section 3). We then plotted the footpoint centroids on the topological maps and looked for a relationship between the spine lines and footpoint tracks. Details of this step is given in Section 4. In Section 5, we propose a evolutionary model to answer two main questions raised by our observations. Firstly, why do the footpoints move along the spine lines? Secondly, does the standard flare model predict the direction and speed of the movement observed?

2. Flare Observations and Analysis

The criteria for the flares chosen in this study were that they occurred within 30 degrees of disk center, were well observed by RHESSI, and exhibited significant footpoint motion. Only a handful of flares fit these criteria, so while compact flares might have been a more simple starting place for this study, all three of the flares we examined were eruptive (as indicated by the Large Angle Spectroscopic Coronagraph (LASCO; Brueckner et al. 1995) coronal mass ejection catalog). These flares occurred on 29 October 2003, 7 November 2004 and 15 January 2005, hereafter A, B and C respectively.

Flare A occurred on 29 October 2003, was observed by RHESSI during all but the decay

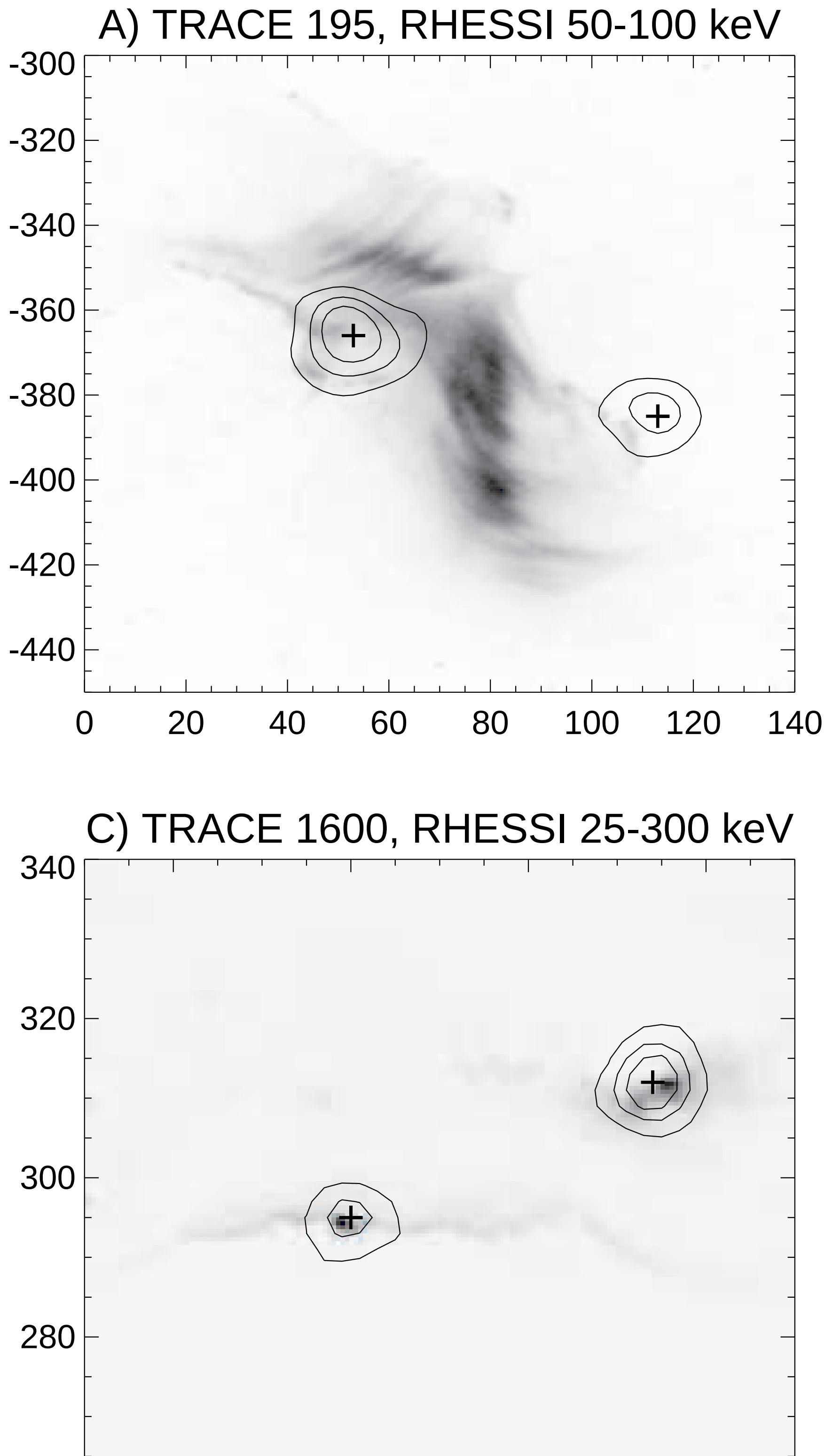

Fig. 1.— TRACE images from flares A and C with RHESSI contours. Top (flare A): TRACE 195 Å image with RHESSI 50-100 keV contours at 30, 50, 70% integrated for 4 s. Bottom (flare C): TRACE 1600 Å image with RHESSI 25-300 keV contours at 30, 50, 70% integrated for 20 s.

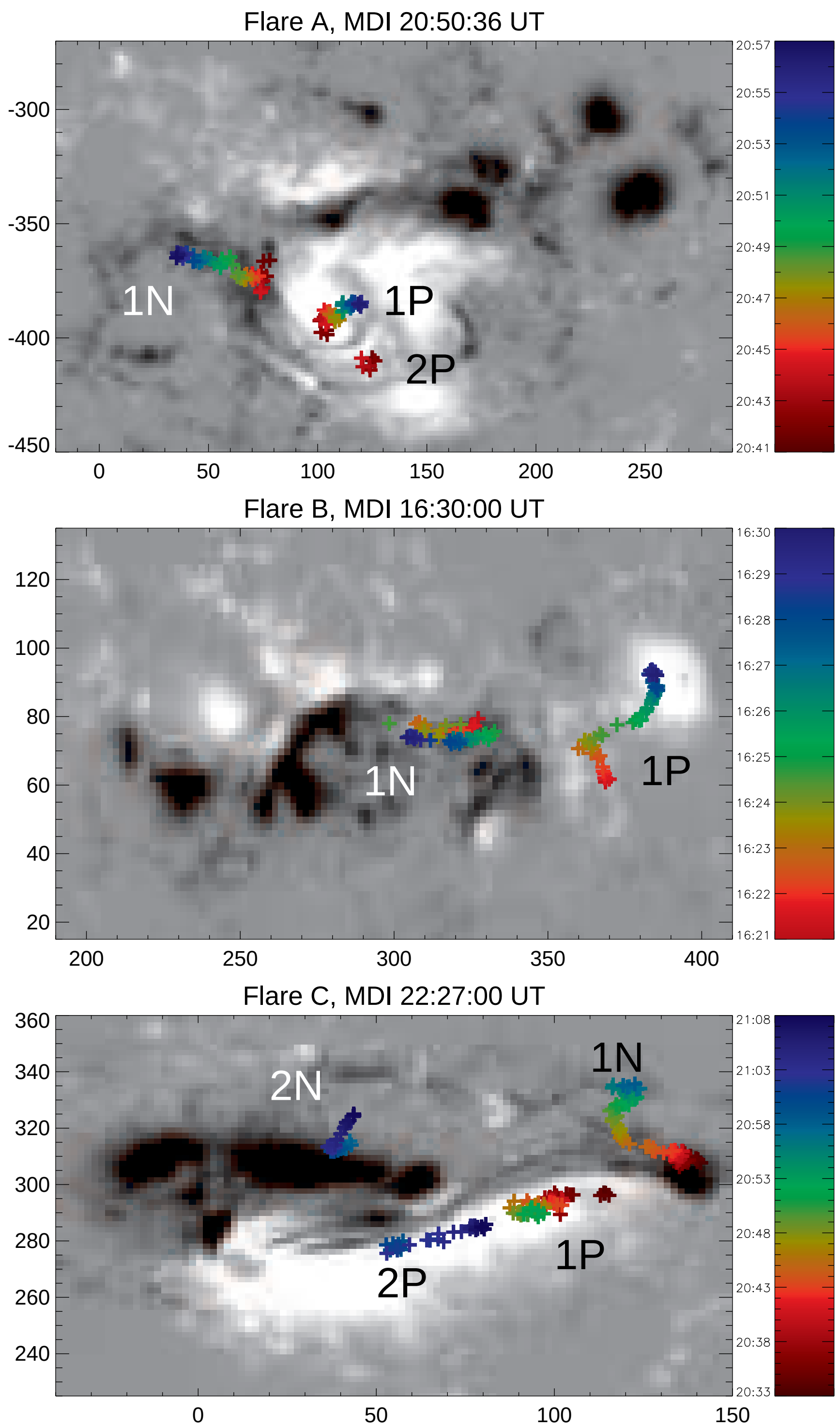

Fig. 2.— MDI line of sight magnetic field images of the three active regions (white is positive, black is negative) and RHESSI HXR footpoint tracks, which follow the color coded UT time scaling shown to the right. Each + symbol marks the centroid location of a source at 50-300, 25-300 and 25-300 keV for flares A, B and C respectively. The centroids are plotted with the following (UT) timing: A - every 20 s from 20:41:00-20:57:00, B - every 10 s from 16:20:50-16:30:00, C - every 20 s from 22:32:40-23:08:20.

Table 1: Flare properties. AR is the active region number and FP motion gives the time range over which the footpoints were observed to move.

Flare	Date	Location (heliocentric ″)	Peak Time (UT)	*GOES* Class	AR	FP Motion (UT)
A	29 Oct 2003	(100, -350)	20:48	X10	10486	20:41-20:57
B	7 Nov 2004	(330, 170)	16:06	X2	10696	16:21-16:30
C	15 Jan 2005	(150, 310)	22:50	X2	10720	22:34-22:58

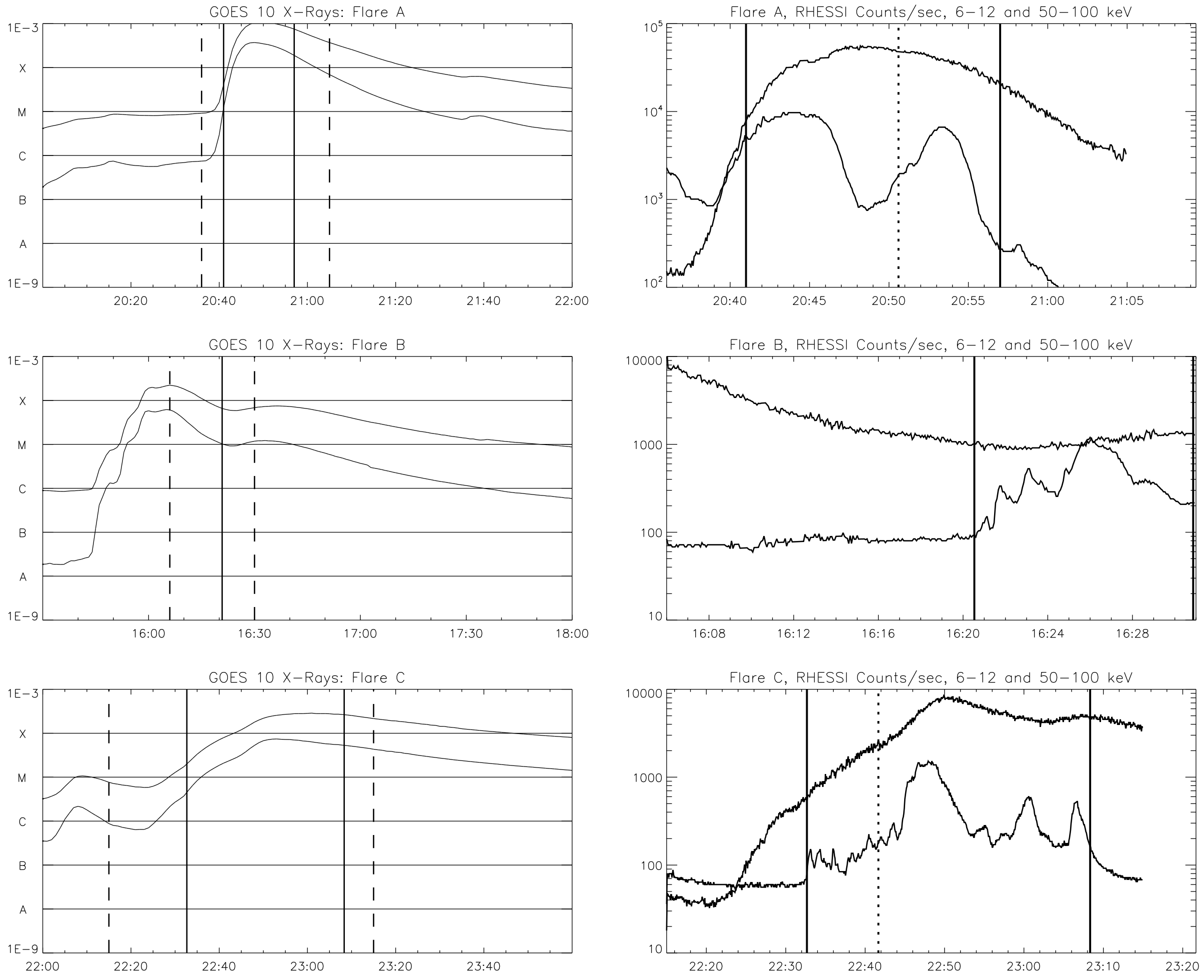

Fig. 3.— Left hand panels are GOES lightcurves for each flare. The dashed lines on the left panels indicate the time range for the right panels. Right hand panels are corrected count rates per second in the 6-12 (top) and 50-100 keV (bottom) energy bins for each flare. In both the right and left panels, the solid vertical lines indicate the time range over which the footpoint motion is observed and plotted in Figures 2. The dotted lines indicate the time of the images shown in Figure 1.

phase and was one of several powerful flares unleashed by the complex active region 10486. Based on images from RHESSI and the Transition Region and Coronal Explorer (TRACE; Handy et al. 1999), we conclude that this two-ribbon flare occurred in a sheared arcade of loops, a portion of which connected two HXR footpoints, shown with contours in Figure 1. Using the RHESSI software's image flux method on data summed over the front segments of all 9 detectors in the energy range 50-300 keV, we calculated the centroid of the footpoint sources every 20s from when they first appeared at 20:41 UT until they faded out at 20:57 UT. The negative polarity footpoint (1N, top panel, Figure 2) moved steadily at $\sim$ 44 km s^{-1} along an extended region of negative flux with average field strength -650 G. The positive footpoint (1P) traveled at a slower rate ($\sim$ 18 km s^{-1}) through a large 1920 G positive source. From approximately 20:41-20:44 UT, a third footpoint source (2P) was present just below and to the east of source 1P. This source exhibited no significant motion during the short time it was observed. Footpoint 1N was present for the entire period while the weaker footpoint 1P was missing for two periods: 20:47:00-20:50:00 and 20:56:20-20:57:00 UT. A substantial decrease in count rate during the first of these periods (see 50-100 keV lightcurve in Figure 3) coincides with a decrease in flux of both footpoints, and footpoint 1P falls below the level of detection.

Flare B was recorded by RHESSI on 7 November 2004 from 16:05-17:04 UT with exception of a span between 16:32 and 16:45 UT. Flare B came right on the heels of an earlier thermal flare just to the west, which occurred mostly during RHESSI night. Both the negative (1N) and positive (1P) polarity footpoints (middle panel, Figure 2) are observed in each of a series of 10 s images from 16:20:50 to 16:30:00 UT. The images were made with the front segments of all 9 detectors in the energy range 25-300 keV. Footpoint 1N takes a curious path through a region with average line of sight field strength -680 G. For the first 2 minutes it moves to the west at $\sim$ 116 km s^{-1}, then travels for 3 minutes to the east before traveling again to the west at a slower rate ($\sim$ 58 km s^{-1}) about 5$''$ below the first westward movement. Footpoint 1P progresses at $\sim$ 80 km s^{-1} along an area of 500 G positive field for about 6 minutes, taking a sharp turn 2 minutes in before slowing down to $\sim$ 18 km s^{-1} in a stronger 1720 G source.

Flare C occurred on 15 January 2005 and was observed by RHESSI during its impulsive phase, from 22:15-23:15 UT. Two sets of footpoints were followed in a series of 20 s images using the front segments of all 9 detectors in the energy range 25-300 keV, starting at 22:32:40 and continuing until 23:08:20 UT. The first set was observed from 22:32:40-22:59:00 UT, where the positive polarity footpoint (1P, bottom panel, Figure 2) disappears from the images after 22:53 UT. A second pair of footpoints (2P and 2N) was detected from 22:58:00-23:08:20 UT. Co-temporal TRACE 1600 Å images (Figure 1) show flare ribbons whose brightest parts are co-spatial with the first set of RHESSI footpoints (1P and 1N). The second set of footpoints was located to the west of the first, the positive polarity footpoint (2P) in the same region of positive flux as 1P, and the negative footpoint (2N) in a separate region from 1N. Footpoint 1P moved slowly ($\sim$ 12 km s^{-1}) through a region with average line of sight field strength 1770 G in a manner that was somewhat random but generally parallel to the nearby magnetic inversion line. Footpoint 1N progressed slowly ($\sim$ 14 km s^{-1}) out of a -1500 G region then moved more quickly ($\sim$ 46 km s^{-1}) through a -670 G area before jumping over to another -290 G source where it did a zigzag across about $10''$ before RHESSI coverage was lost. The later set of footpoints, 2P and 2N, moved along a 1620 G extended source at $\sim$ 37 km s^{-1} and moved to the boundary of a -620 G region at $\sim$ 50 km s^{-1}, respectively. Due to its location, we hypothesize that the second set of footpoints was from a separate sympathetic flare. Further evidence for this hypothesis can be observed in the RHESSI lightcurves (Figure 3). At 22:58, when the second set of footpoints appears, the flux observed in the 6-12 keV energy band is decreasing, a sign that the first flare is decaying. However, the HXR emission (50-100 keV) continues for another 10 min and the 6-12 keV emission rises to a second peak. These factors led us to conclude that footpoints 2P and 2N were part of a sympathetic flare.

When discussing footpoint movements, one of the first steps to take is to establish footpoint conjugacy. We have done this using three techniques. First, we compare the general characteristics (e.g. start, peak and end times) of the HXR light curves of the candidate pair. If the two footpoints are connected by the same field lines, then the fast electrons running down either side of those lines should impact the chromosphere at approximately the same time. With a 20 s imaging cadence, the sources' light curves should coincide. Second, we examine the MCT model topology to see if a connection exists between the positive and negative magnetic sources associated with the footpoints. Third, if an extreme ultraviolet image is available during the flare time, we look for a hot loop connecting the HXR source regions. This visual connection gives credence to hot evaporated plasma having filled up the newly reconnected loop. The employment of these techniques leads us to the conclusion that the HXR sources 1P and 1N of flare A are conjugate. Due to a lack of extreme ultraviolet images during flare B, the case for conjugacy is not as strong. However, the RHESSI data and topology lend enough support that we claim sources 1P and 1N of flare B are conjugate. Flare C has two sets of conjugate footpoints: sources 1P and 1N and sources 2P and 2N.

As a side note, we remark on an interesting observation involving the magnetic field strength associated with the HXR footpoint sources and the footpoint speeds. An anti-correlation between field strength and average footpoint speed was found to be significant at the 90% level via the calculation of the Kendall coefficient. The average speed of sources with underlying field strengths of less than 1000 G is $\sim$ 59 km s^{-1} while the average speed for those with strengths of more than 1000 G is $\sim$ 19 km s^{-1}. The relationship between field strength and footpoint speed has been noted before, most recently by Krucker et al. (2005). Although we find this observation intriguing, will not analyze it further in this paper.

3. Topology Observations and Analysis

In order to understand the topological location of magnetic reconnection, we need to characterize the connectivity of the field. An approximation must be made in order to produce the boundaries needed to determine this connectivity. Here, we approximate the field by using a MCT model. Following Longcope & Klapper (2002), the line-of-sight field recorded in magnetograms is partitioned into strong-field regions. Each region is then characterized by a point source which matches the region's net flux and is located at the region's centroid.

In the standard 2.5D model for two-ribbon flares, the CSHKP model (Carmichael 1964; Sturrock 1968; Hirayama 1974; Kopp & Pneuman 1976), the footpoints are predicted to move apart from one another as the reconnection region moves higher in the corona. As field lines are reconnected, the footpoints travel across continuous regions of magnetic flux. In the MCT model, this flux region is represented by a point source, so we cannot follow a footpoint path across it. We can, however, use the concept of spine lines to make the connection between footpoint motion and the MCT model. Spine lines extend across strong-field regions, providing paths through regions of like flux that can be compared to the paths traveled by the HXR footpoints.

As with any coronal field extrapolation model currently available, there are limitations to the MCT model we use. One limitation of our model is the loss of information on the geometry of the field. This is a result of representing patches of magnetic field with point sources. We cannot distinguish if a coronal field line emanates from the outside edge of the modeled source or the center. We are not concerned, however, with the exact location of the topological features of the field – the geometry – but are only interested in the connectivity.

Another limitation of this extrapolation model is that it is potential. Currently, we do not have the ability to model coronal fields above the complex active regions where flares typically occur with a non-linear force free field model. Nevertheless, a moderately stressed field probably has a topology similar to that of the potential field (Brown & Priest 2000); it has the same separators dividing the flux domains and the same spines modeling photospheric sources.

A third limitation of this MCT model is our inability to consider open field lines or sheared or twisted flux tubes, whose currents can induce significant topological changes. This means that we cannot say anything about the properties of the flux tube which becomes the coronal mass ejection in the CSHKP model. The evidence we have for reconnection deals with electrons streaming along the closed field lines that have collapsed down beneath the separator. Using these closed field lines and the information we have from HXR emission still allows us to point to the topological location of reconnection and thus learn a great deal about the release of energy in flares.

Topological models can be applied more directly to eruptive flares by following flux changes in the strong field regions during the tens of hours prior to a flare. This has been done by Longcope et al. (2007) for the 7 November 2004 X2 flare using the Minimum Current Corona model (MCC; Longcope 1996, 2001). While calculating the MCC model certainly has quantitative advantages, it is beyond the scope of this paper.

The MCT model produces a topological map at the photosphere which can be used to extrapolate the field into the corona. The calculation of the topology begins by selecting a subregion, namely the main body of the active region, from full-disk MDI magnetograms made as close to the flare start time as is available, typically within 30 min. Next, the observed field is partitioned by grouping pixels that exceed a set threshold (100 G for flares A and B, 50 G for flare C) and are downhill from the local maximum into a region. Regions with fewer than 10 pixels are discarded.

The partitioning determines the location and charge of each pole. A potential field extrapolated from these determines the locations of the nulls. Once the nulls are calculated, the spine lines, separatricies and separators are given by the physics of the MCT model.

The skeleton *footprint*, the intersection of the separatrix surfaces with the photosphere as well as the spine lines, poles and nulls, characterizes the topology of the model and shows the connectivity of the field visually. The area within a domain's boundary, formed in part by the intersection of the separatricies with the photospheric plane and in part by the spine line, contains the photospheric footprint of the set of field lines connecting the domain's positive and negative poles. The topological footprint for flare A is given in the top panel of Figure 4. Source P01, pointed out by the arrow, is connected to many negative sources, including N22, N14, N08 and N13, which are just to the east of P01. For clarity, subsequent figures show only the poles (unlabeled), nulls and spine lines.

We paid careful attention to the co-alignment of the MDI magnetograms and RHESSI data. Spatial alignment of MDI and RHESSI data taken at the same time typically agree to within $2''$ (Krucker et al. 2005). The MDI magnetograms are differentially rotated to the midpoint time of the observed footpoint motion to ensure the best spatial and temporal comparison. One of the criteria for topological analysis of this type is that the flaring region not be more than about 30 degrees from disk center. Outside of 30 degrees, the line-of-sight component of the field is not an accurate enough approximation for our topological models.

Topological analysis gives the connectivity of the field, which is important in this study for two main reasons. One, it aids in the determination of conjugate HXR footpoints. If two HXR sources are conjugate, then there must be field lines connecting the corresponding magnetic sources. Two, the connectivity gives the locations of topological features such as spine lines, which, as we argue in this paper, are important analytical tools in the study of reconnection and particle acceleration in flares.

4. Analysis of Footpoint Motion and Spine Lines

While analyzing the topology of active region 10486 with respect to the HXR footpoints of flare A, we noticed a remarkable visual relationship between the spine lines and footpoint tracks. For example, track 2 (top panel, Figure 5) moves through an extended region of negative flux nearly parallel to the spine line. We then expanded our analysis to two different flares, flares B and C, and observed the same relationship. In flare B (center panel, Figure 5), the footpoint associated with the positive magnetic field makes two turns, from track 2 to 3 and from track 3 to 4, which resemble the spine line curves. As in the first case, the footpoint is moving along an elongated area of flux. The spine lines trace through this flux, connecting a source to an intermediate null

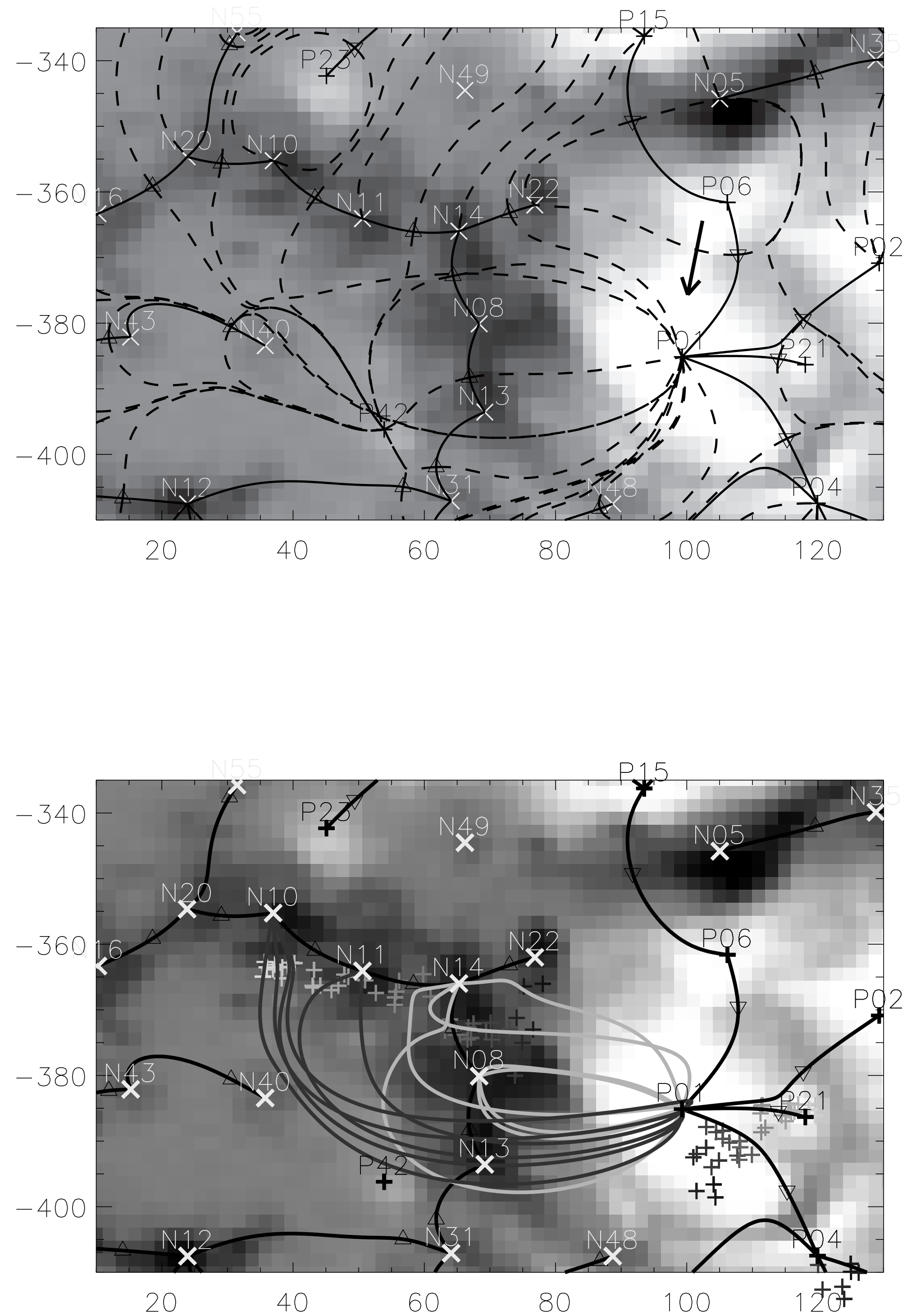

Fig. 4.— Top: photospheric footprint of the topology for flare A. P markers (+) are are positive poles while N markers (×) are negative poles. The triangles are null points, either positive (▽) or negative (△). Solid lines are the spine lines and dashed lines are the intersection of the separatrix surfaces with the photosphere plane. The arrow points out pole P01, which is used in an example in Section 3. Bottom: example field lines for flare A.

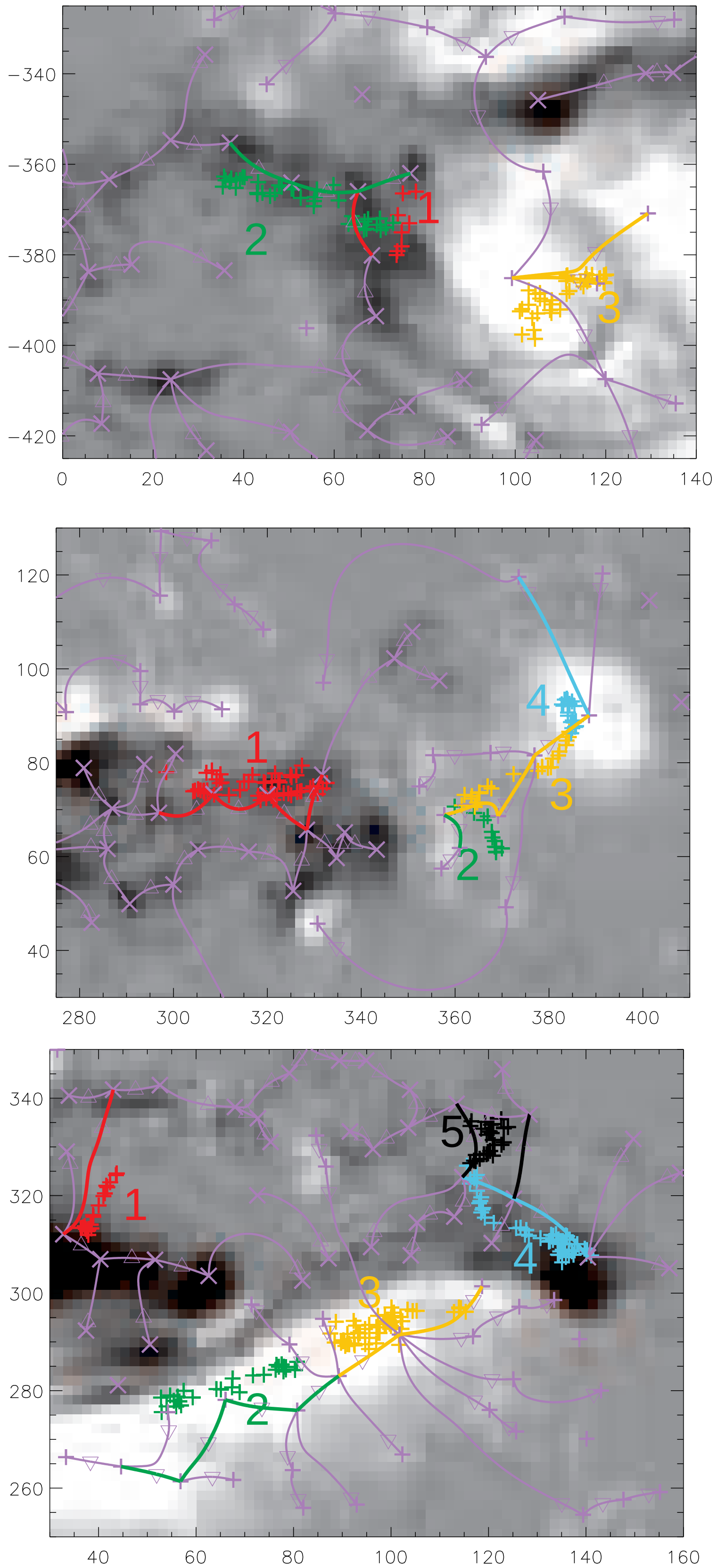

Fig. 5.— Poles, nulls, spine lines and footpoint tracks on magnetograms for flares A (top), B (center) and C (bottom). Violet lines are spine lines which we did not associate with footpoints. Spine lines marked with non-violet colors were identified (and quantitatively analyzed) with the footpoint tracks of like color.

to another source. Notice also that this footpoint slows down once it reaches the strong positive region of flux at the end of its path.

Not all footpoint tracks have shapes identical to the corresponding spine line. For example, track 2 of flare C (bottom panel, Figure 5) moves in a nearly straight path along the main region of positive flux, while the spine line, due to the locations of the nulls, makes a W shape. This discrepancy can be explained by the nature of the topological approximation. As we discussed in Section 3, information about the geometry of the magnetic field is lost in the process of defining the field's connectivity. The loss of information occurs when boundaries are drawn around source regions and the source regions are represented by point charges. Thus, the location of the spine lines have a spatial uncertainty proportional to the size of the source region. The larger the source region, the larger the uncertainty in the location of spine line. The defining property of a spine line is that it connects regions of like flux. Depending on the characteristics of local maxima in the field, a spine line can take on different paths through the flux regions. We refer again to track 2 of flare C. Here, the spine line reflects the structure of the positive field, but the HXR footpoint simply moves through it.

In order to quantify the association of spine lines and HXR footpoints of the type described above as well as those with a clear visual relationship, we conducted an analysis of the two features' average angles. Due to the nature of the uncertainties in the spine lines, the angle at which the footpoints moved relative to the spines is more important than their distance from the spine lines.

The HXR footpoint angles shown in Table 2 were calculated by finding the angle between consecutive centroids and averaging these angles for each footpoint track. Angles were measured from 0 to 2π radians where 0 rad. always pointed straight to the right of footpoint centroid i. If centroid $i + 1$ was located directly north of i, then the angle between these footpoints was $\pi/2$. A footpoint moving straight from right to left would have the average angle π. In some cases, footpoints did move steadily in one direction and thus the standard deviation of the angles was small (~ 0.3 rad). However, in other cases, footpoints moved more randomly and the uncertainty was larger (as large as 1.23 rad.). By integrating over more time when reconstructing RHESSI images, we could have smoothed over some of the small spatial variations. Nevertheless, we wanted to retain a much spatial and temporal information as was allowed by count statistics.

Spine line angles were calculated with the same method as the footpoint tracks, averaging the angles from one point on the spine curve to the next. The uncertainty in the spine angle comes from the fact that a spine can extend from a null at the edge of a flux region across the region in any direction. In our method, the pole is placed at the region's center of flux, such that the spine extends from the null through the center. However, in the un-approximated field the spine line, as an edge of a domain, can extend across the region from the null through any point in the region. Thus, the uncertainty in the spine angle is proportional to the width of the region. To calculate this uncertainty, we measured the angular width of each flux region by finding the angle between two special lines, one drawn from a spine's null to the widest point of the flux region and the other from the spine's null to the center of flux.

Once we calculated the two sources of error – the standard deviation of the footpoint angle and the uncertainty in the spine line angle(s) – we added them in quadrature to produce a total uncertainly. We then checked if each average spine and footpoint angle agreed to within the total uncertainty. Not only was it confirmed that the two angles agreed with each other in every case, but they often matched much more closely than the total uncertainty angle. This can be explained by the fact that our method gives the maximum total error. If we had simply fit the footpoint track with a line and found how well each HXR centroid agreed with this line, our error would have been smaller. The best fit line method, however, doesn't accurately represent the detailed motion of the footpoints; it smoothes out the short time-scale variations.

Table 2 gives the spine line and footpoint track angles as well as their differences. If the spine lines and footpoint tracks were unrelated and their angles were random, then the distribution of their differences would be flat. The distribution is *not* flat, but peaks about 0. Differences in the two angles extends between 0 and $\pi/2$ because spine lines have no temporal 'direction'. We chose to calculate the spine angles in the same direction as the footpoint motion. Thus, the largest the angle differences could have been is $\pi/2$ rad.

In order to quantify the significance of this result, we applied the Kolmogorov-Smirnov (K-S) test (Press et al. 1992) to the unbinned angle differences. The K-S test is the best test for our sample because it assumes nothing about the distribution and uses no bins, both of which can affect the accuracy of other tests. We find that we can reject the null hypothesis that the average spine line and footpoint track angles have a random relationship with 99.95% confidence. Therefore, it is our observational conclusion that the RHESSI HXR sources move along spine lines.

5. Discussion

In this paper, we have demonstrated the association of HXR footpoint tracks and spine lines. Now the question is *why* the HXR footpoints move along spine lines. To understand this relationship, we first need to examine the types of footpoint motion commonly observed. Somov et al. (1998) define two categories of flares: more impulsive and less impulsive, acknowledging that some flares are of an intermediate type. They state that in more impulsive flares, which have impulsive phases lasting less than 30-40 s, the HXR footpoints move toward one another. Less impulsive flares, with impulsive phases lasting longer than 30-40 s, undergo an increase in the distance between footpoints. Others (i.e. Bogachev et al. 2005) refer to footpoint motion using descriptions such as motion parallel or perpendicular to the magnetic inversion line.

In the standard 2.5D model for two-ribbon flares, the CSHKP model, the footpoints are predicted to move apart from one another as the reconnection region moves higher in the corona. This separation can only occur *perpendicular* to the magnetic neutral line. The footpoint separation velocity predicted in the standard model is a only few km s^{-1}(Somov et al. 1998). Actual velocities observed by the *Yohkoh* HXT and RHESSI are much larger, on the order of $\sim$ 50 km s^{-1} (see Section 2). Also, the standard model cannot explain footpoint motion with no or decreasing separation, as is often observed (i.e. Sakao et al. 1998). To account for the observed motions and their separation speeds, a 2 or 2.5D model is inadequate; a 3D model is needed. Here, we present such a model, which is an evolution of the 2D CSHKP model into a 3D topological model.

The motion and speed of footpoints along spine lines can be understood with the aid of the quadrupolar model in Figure 6. Even in the most complex field, each individual reconnection event involves only 4 domains and therefore can be understood in terms of a quadrupolar configuration. The quadrupolar configuration is not meant to model the entire flaring region, but rather, the separator in the configuration is one of several on which reconnection occurs over the course of a flare.

We discuss three cases of reconnection events for this quadrupolar model. In each case, reconnection is the result of a flux imbalance in part of the quadrupolar configuration. As a flare progresses, the reconnection moves from separator to separator (thus from one quadrupolar region to another), balancing the flux and reducing the energy state of the magnetic field.

The assumptions involved in our explanation include the following. Reconnection occurs at a current sheet which is located on the separator, producing fast-precipitating electrons which stream along the separator field line until they encounter the chromosphere. At the chromosphere, the electrons are decelerated via thick-target bremsstrahlung, resulting in the HXR footpoint sources.

We point out that linked spine lines are the topological characterization of extended regions of like flux. The MCT extrapolation model's point sources (poles) represent patches of photospheric flux. The poles are placed at patch's center of flux. Between two poles exists a place where the field strength goes to zero (a null). A single spine line connects two like poles via the null. Often, a spine line links not just one pair of poles, but continues to another null and then another pole, and so on. It is not surprising, therefore, that the HXR footpoints move along the spine lines, especially in the cases where the magnetic flux is strung out in fragmented pieces as in track 2 of flare A. The correlation, however, between spine lines and non-fragmented flux is also significant. For example, track 3 of flare C, which extends through a solid area of flux, corresponds to the spine line to within 0.18 rad.

In case 1, we suppose that the domain P2/N2 (containing the red field lines) has too much flux in the sense that it can reach a lower energy state (become more potential) by decreasing its flux through reconnection. Also, let's say the separator in the figure is at the position drawn at time t=0. If a field line from the underlying flux domain P2/N2 approaches a field line in the overlying domain P1/N1 at the separator and reconnects, producing two new field lines in the domains P2/N1 (orange) and P1/N2 (purple), then the reconnected flux is moved from P2 into P1 and from N2 into N1. At a later time t=1, the separator is located closer to the P2 source center due to P2's loss of connecting field lines and P1's gain. The other end of the separator is closer to N2's center due to N2's loss and N1's gain. As time goes on, the process of P2 losing field lines

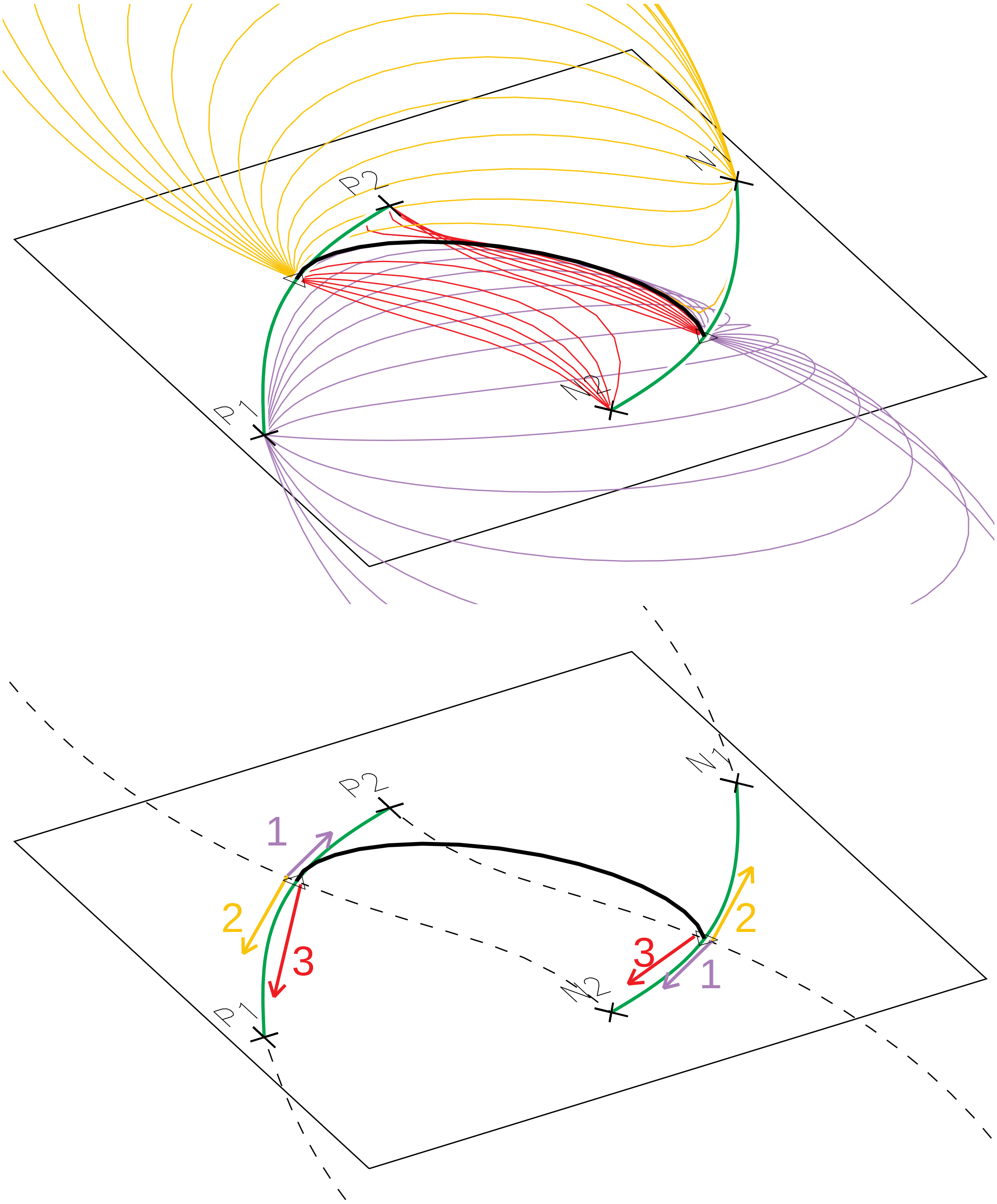

Fig. 6.— Upper panel: key topological features. P2 and P1 (+) are are positive poles while N1 and N1 are negative poles (×). The triangles are null points, one positive (▽) and one negative (△). The orange, purple and red field lines lie on the separatrix surface under which exist all of the field lines connecting P2/N1, P1/N2 and P2/N2 respectively. Above the orange and purple separatricies is the domain containing all of the field lines that connect P1 to N1. All four of these domains intersect at the separator (thick black line). The thick green lines are the spine lines. Lower panel: expected footpoint movement along the spine lines for the configuration in the upper panel. Dashed lines are the intersections of the separatrix surfaces with the photosphere. Arrows indicate the direction of separator movement during reconnection for cases 1, 2 and 3 (see Section 5).

to P1 and N2 to N1 continues, and the chromospheric ends of the separator (and hence the HXR footpoints) move antiparallel and slightly *toward* each other along the spine lines, shown by arrows in Figure 6.

Somov et al. (1998) present a different analysis reaching a similar conclusion. In their topological model 'more impulsive' flares have decreasing longitudinal magnetic flux along the separator, resulting in a decrease in the distance between footpoints. They also point out that the reconnected field lines decrease in length as the reconnection process proceeds. This is the same basic physical process we describe in case 1, with the exception that we refer specifically to how the *separator* changes rather than the decrease of longitudinal flux and reconnected field line length. In case 1, the separator would shorten in length and decrease in height as the domain beneath it shrank.

In case 2, we suppose that the domain P2/N2 (red) has too little flux, so field lines from the domains P1/N2 (orange) and P2/N1 (purple) reconnect to form new lines in P1/N1 and P2/N2. Here, the footpoints move towards the N1 and P1 centers of flux, antiparallel and *away* from each other along the spine line. The separator lengthens and increases in height as the domain beneath it grows.

This example is similar to the reasoning used to explain two ribbon flares with sheared arcades. When a sheared magnetic field suddenly releases energy in the form of a two ribbon flare, domains of source pairs initially far apart and nearly empty of flux now have too little flux relative to a lower-energy field. In order to lower the energy state, flux is added to the underlying deficient domains, reducing the shear in the field and increasing the length and height of the separator. The separator current sheet moves along the spine lines, sweeping through equal areas of positive and negative photospheric flux and the flare footpoints move apart. The magnetic sources themselves don't change–only their connectivity does so.

In case 1 the imbalance of flux led to the growth of both center domains P1/N2 and P2/N1 (purple and orange) and case 2 led to their shrinkage. In case 3, we deal with the final possibility of flux transfer in a quadrupolar configuration – when there is a flux imbalance in one of the center domains with respect to the other. For example, we assume the domain P1/N2 has to much flux and it can reach a lower energy state by transferring flux from domains P1/N2 (purple) and P1/N1 (overlying) into domains P2/N1 (orange) and P2/N2 (red). In this process, the entire separator shifts along the magnetic neutral line as the footpoints move *parallel* to each other towards the P1 and N2 poles. Parallel HXR footpoint motions are often observed; for example, Bogachev et al. (2005) report that 35% of the flares they observed had HXR footpoint sources that moved in the same direction.

To summarize, footpoint motion along spine lines corresponds to movement of the reconnection location. As the separator current sheet sweeps across region of flux, its chromospheric ends either move toward each other (compact flare; case 1) as the separator shortens, the ends move away from each other (eruptive two ribbon flare; case 2) as the separator lengthens or the ends move parallel to each other (case 3) as the separator stays approximately the same length. The movement of the separator's chromospheric ends, and hence the HXR footpoints, is along the spine lines. Spine lines connect two poles via a null which shifts during the flare toward one pole or the other. The direction the null shifts depends on the global configuration of the region; the underlying domain gains or loses flux in order to decrease the region's energy state.

The above explanation agrees with the observed footpoint tracks and footpoint separation speeds of the three flares reviewed in this paper. Referring again to Figure 4, we propose the following explanation for the footpoint motions of flare A. As is indicated by the number of light grey field lines drawn in domains P01/N14 and P01/N08, a large percentage of P01's flux is connected to N14 and N08. Initially, the footpoint separation distance decreases due to the reconnection of flux out of underlying domains P01/N14 and P01/N08. The next stage of reconnection acts to release energy stored in the sheared arcade. Domains which have little connecting flux in the earlier stage of the flare (P01/N11 and P01/N10) fill up as reconnection takes place on higher and longer separators, and the footpoints move apart from one another. An in-depth analysis of separator properties before and after flares will be given in a subsequent paper.

Our model can be compared to other models that have been proposed to explain HXR footpoint source motions. Bogachev et al. (2005) use a sheared 2.5D model to explain the antiparallel motion of HXR footpoints along the neutral line. In their model, which cannot distinguish between flares with increasing footpoint separation from flares with decreasing separation, the apparent motions of HXR sources are determined by the order of reconnection along the sheared system of field lines. During the onset of a flare, the footpoint sources move toward each other, decreasing the distance between them, until a critical point is reached and the sources begin to move away from one another. This model is similar to other models of reconnection in sheared arcades, where reconnection starts on the most highly sheared field lines and progresses to the less sheared field higher in the corona. As was pointed out earlier in this section, case 2 of our model is analogous to these models where reconnection in sheared fields leads to the antiparallel motion of HXR footpoint sources. In this case, the flux deficiency in the underlying domains, due to the shear in the initial configuration, leads to reconnection that increases the length of the separator, and consequently, the footpoint separation increases.

Our model is also comparable to the slip-running reconnection model proposed by Aulanier et al. (2006), which describes reconnection within the framework of QSLs. In complex 3D magnetic configurations, QSLs become separatrices as their width approaches zero. In fact, the intersection of QSLs with the chromosphere are similar to spine lines in that they extend from one magnetic flux source to another of the same polarity. Within the QSL, the sub-region where the squashing degree Q (Titov et al. 2002) peaks (where the connectivity gradients are the largest) is known as the hyperbolic flux tube (HFT; Titov et al. 2003). A HFT becomes a separator as its squashing degree asymptotically tends to infinity. Aulanier et al. (2006) state that QSL reconnection leads to field line slippage along the QSLs and thus the field lines slip-run along the intersection of the QSLs with the line-tied boundary. In this reconnection process, particles are accelerated to their highest energies in the HFT, so HXR emission is expected at the chromospheric ends of the HFT.

Given this and the fact that the intersection of the QSLs with the chromosphere correspond to flare ribbons (e.g. Démoulin 2006), slip-running reconnection is a possible explanation for the motion of HXR sources along flare ribbons. Due to the analogies between the intersection of QSLs with the chromosphere and spine lines, as well as between HFTs and separators, we suggest that slip-running reconnection is the QSL version of the separator reconnection modeled in this paper.

The association of footpoints tracks with spine lines, and more importantly the physical explanation for the association, can be used in future flare analysis. Having an explanation for why HXR footpoints move the way they do will aid in the understanding of flare initiation and evolution. Further work with topological models, especially analysis involving the role separator current sheets, is needed to understand this and other aspects of the flaring process.

This work was supported by RHESSI funds from the University of California at Berkeley through a contract, SA1868-26308PG, with Montana State University. Funding for our Research Experience for Undergraduates (REU) students was provided by NSF grant ATM-0243923.

REFERENCES

Aulanier, G., Pariat, E., Démoulin, P., & Devore, C. R. 2006, Sol. Phys., 238, 347

Bogachev, S. A., Somov, B. V., Kosugi, T., & Sakao, T. 2005, ApJ, 630, 561

Brown, D. S., & Priest, E. R. 2000, Sol. Phys., 194, 197

Brueckner, G. E., et al. 1995, Sol. Phys., 162, 357

Carmichael, H. 1964, in The Physics of Solar Flares, ed. W. N. Hess, 451

Démoulin, P. 2006, Advances in Space Research, 37, 1269

Fletcher, L., & Hudson, H. S. 2002, Sol. Phys., 210, 307

Gorbachev, V. S., & Somov, B. V. 1988, Sol. Phys., 117, 77

Greene, J. M. 1988, J. Geophys. Res., 93, 8583

Handy, B. N., et al. 1999, Sol. Phys., 187, 229

Hirayama, T. 1974, Sol. Phys., 34, 323

Kopp, R. A., & Pneuman, G. W. 1976, Sol. Phys., 50, 85

Kosugi, T., et al. 1991, Sol. Phys., 136, 17

Krucker, S., Fivian, M. D., & Lin, R. P. 2005, Advances in Space Research, 35, 1707

Lau, Y.-T., & Finn, J. M. 1990, ApJ, 350, 672

Lin, R. P., et al. 2002, Sol. Phys., 210, 3

Longcope, D. W. 1996, Sol. Phys., 169, 91

Longcope, D. W. 2001, Phys. Plasmas, 8, 5277

Longcope, D. W. 2005, Living Reviews in Solar Physics, 2, 7

Longcope, D. W., Beveridge, C., Qiu, J., Ravindra, B., Barnes, G., & Dasso, S. 2007, Sol. Phys., in-press

Longcope, D. W., & Klapper, I. 2002, ApJ, 579, 468

Metcalf, T. R., Alexander, D., Hudson, H. S., & Longcope, D. W. 2003, ApJ, 595, 483

Press, W. H., Teukolsky, S. A., Vetterling, W. T., & Flannery, B. P. 1992, Numerical recipes in C. The art of scientific computing (Cambridge: University Press, —c1992, 2nd ed.)

Sakao, T., Kosugi, T., & Masuda, S. 1998, in ASSL Vol. 229: Observational Plasma Astrophysics : Five Years of YOHKOH and Beyond, ed. T. Watanabe & T. Kosugi, 273

Scherrer, P. H., et al. 1995, Sol. Phys., 162, 129

Somov, B. V., Kosugi, T., & Sakao, T. 1998, ApJ, 497, 943

Sturrock, P. A. 1968, in IAU Symp. 35: Structure and Development of Solar Active Regions, ed. K. O. Kiepenheuer, 471

Titov, V. S., Galsgaard, K., & Neukirch, T. 2003, ApJ, 582, 1172

Titov, V. S., Hornig, G., & Démoulin, P. 2002, Journal of Geophysical Research (Space Physics), 107, 3

Table 2: Footpoint track and spine line average angles and their difference.

Flare, Track	Footpoint Angle	Spine Angle	Difference
A, 1	4.13	4.95	0.82
A, 2	3.31	2.96	0.35
A, 3	0.69	0.29	0.40
B, 1	3.34	3.36	0.02
B, 2	2.67	2.00	0.67
B, 3	0.70	0.68	0.02
B, 4	2.20	2.04	0.16
C, 1	1.65	1.23	0.42
C, 2	0.64	0.41	0.23
C, 3	3.51	3.69	0.18
C, 4	2.55	2.55	0.00
C, 5	1.09	1.49	0.40